Linear and Nonlinear Wave Propagation in Booming Sand Dunes

N. M. Vriend,[1] M. L. Hunt,[2] and R. W. Clayton[3]

[1)] *Department of Applied Mathematics and Theoretical Physics, University of Cambridge, Cambridge CB3 0WA, UK.*[a)]

[2)] *Division of Engineering and Applied Science, California Institute of Technology, Pasadena, CA 91125, USA.*

[3)] *Division of Geological and Planetary Sciences, California Institute of Technology, Pasadena, CA 91125, USA.*

(Dated: 11 September 2015)

The current field study examines linear and non-linear acoustic waves found in large desert sand dunes using field measurements of wave speed, frequency content, dispersion, and polarization. At the dune fields visited, an avalanching of sand can trigger a loud booming or rumbling sound with narrow peak frequencies centered between 70 and 105 Hz with higher harmonics. Prior to the onset of the nearly-monotone booming, the emission consists of short bursts or burps of sound of smaller amplitude and over a significantly broader range of frequencies. These burps have similar frequency content to sounds generated by small scaling shearing at a dune site or in laboratory-scale experiments.

By investigating the wave characteristics of both burping and booming emissions, this manuscript demonstrates that booming and burping correspond with the transmission of different waves within the dune. The burping sounds correspond to a surface Rayleigh wave with nonlinear and dispersive properties. The booming emission results from a linear, non-dispersive P-wave, which supports an earlier analysis where booming is modeled as the trapping of the body waves in the dune's surficial layer. Besides characterizing the booming and burping emissions, this manuscript illustrates the effect of scale in the wave propagation of granular materials, when non-linear, dispersive waves across small scales transition to linear, non-dispersive waves across larger scales.

PACS numbers: 45.70.Mg, 45.70.Ht, 81.05.Rm

[a)] Previously at the Division of Engineering and Applied Science, California Institute of

Technology, Pasadena, CA 91125, USA.; Electronic mail: n.m.vriend@damtp.cam.ac.uk; http://www.damtp.cam.ac.uk/user/nv253/

I. INTRODUCTION

In certain locations around the world, large (heights $\geq 30\,\mathrm{m}$) sand dunes can generate a sustained (up to several minutes) booming or rumbling emission after a sand avalanche[1,2]. In prior studies, this desert sound has been described as a "rumble of distant thunder when the soil is in violent oscillation"[3], a "hum" and "might be likened to the noise made by an aeroplane at a distance in steady flight"[4], "throaty booming"[5], and "emissions similar to a didgeridoo with its low, droning cadence"[6]. The frequency content of the booming sound consists of a primary frequency between 70 and 105 Hz (with frequency width at mid-height less than 10 Hz) plus higher harmonics. This emission occurs most frequently in the hot and dry summer months. In the wetter season, the in situ sustained booming is difficult, if not impossible, to create suggesting that factors beyond the properties of the sand grains determine whether booming can occur[6].

In the current work, the field measurements are made at two different field sites: Eureka Dunes in Death Valley NP and Dumont Dunes in the Mojave Desert, California, USA; these sites are approximately 270 km apart and are described in greater detail in Vriend, Hunt, and Clayton[7]. Figure 1 shows a 32 s sample of data from a geophone embedded within an avalanching region of Eureka Dunes along with the frequency spectra measured during the first 1 to 3 seconds and from 15 to 17 seconds. During the initial 1 to 3 seconds, the signal contains short bursts or "burps" and a broadband signal between 50 to 90 Hz; after approximately 5 seconds, the signal strength increases significantly as found in the voltage-time plot. Between 15 to 17 seconds, the booming frequency is concentrated between 80 to 90 Hz with higher harmonics. During this entire time period, the individuals sliding down the dune moved from above to below the embedded geophone in the downhill direction.

Similar burping and booming signals from large sand dunes have been obtained on multiple trips to both Eureka and Dumont Dunes with both natural and man-made avalanches; in addition, similar data are also found when the geophone is placed in the dune but outside the avalanching region. In Vriend *et al.*[8], the authors show that the monotone booming cannot be generated on smaller dunes within the same dune field that have similar sized sand grains; however, the avalanching of sand generated a lower-amplitude broad-band signal that is comparable with the burping sound shown in Figure 1. In a paper by Dagois-Bohy, Courrech du Pont, and Douady[9], the authors present a similar frequency spectrum using a

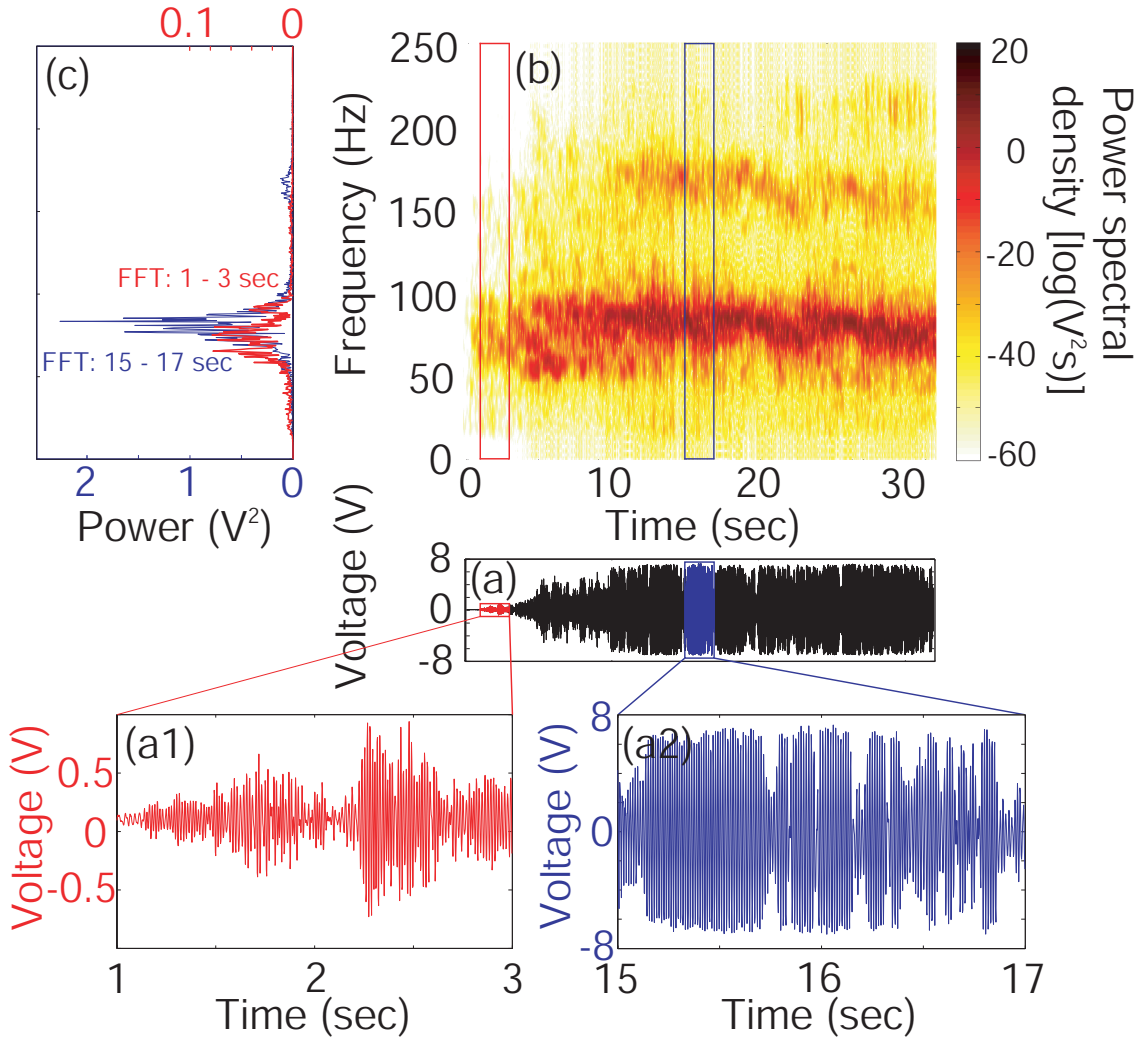


FIG. 1. A slide generated on Eureka Dunes on 10/27/2007, featuring short bursts of sound, or "burping" in the beginning of the slide and sustained "booming" emissions in the latter parts of the slide. (a) Voltage signal recorded for 32 seconds from a geophone deployed in the sand; the voltage is significantly lower for the burping emission—panel (a1)—in the beginning of the recording compared to the booming emission—panel (a2)—in the middle and latter part of the recording. (b) Spectrogram of the geophone recording, showing the power spectral density as a function of time (32 s) and frequency content (up to Nyquist frequency 250 Hz)—a main frequency with a higher harmonic exists for the booming emission. (c) Fast Fourier Transform over 3 seconds for the burping emission (red, 1 – 3 s), showing a broad frequency content, and the booming emission (blue, 15 – 17 s), illustrating a factor 20 larger power.

microphone for a megabarcan dune in Morocco; the signal included in the paper showed a

similar lower-amplitude, lower-frequency burping emission prior to the monotone booming at 100 ± 5 Hz. This paper also includes spectra from a smaller "singing" barchan dune in Al-Askhara, Oman. According to the authors, the dune "sings" but there is no dominant frequency; instead the spectra show burps of sound with frequencies from 50 to 150 Hz.

In this study, the term "burping", is used but other researchers have described the sound as "moaning sounds"[3], "roars"[4], "thrums"[5] and short "squeaks"[6]. Several prior studies have also shown that well-rounded, smooth, desert sand can produce pulse-like burps by local shearing, such as by moving a hand, shovel or boot[10] quickly along the booming dune surface. Burping sounds may be generated by shearing or shaking a small sample of dune sand in a jar or bottle[5]. Similar broadband sounds have also been recorded in the laboratory using a rotating bed moving past a fixed paddle[11,12]. Douady *et al.*[11] and Dagois-Bohy, Courrech du Pont, and Douady[9] observed that the frequency of burping sounds depends on the shear rate and the particle diameter of the sample.

The focus of this paper is to characterize the waves associated with the booming and burping sounds by measuring not only the frequency spectra but also the wave speeds and attenuation. Prior studies of booming dunes have associated the sounds with both surface and body waves. Andreotti[13] used two sensors and an external excitation and measured the dispersive properties of a sound wave through sand with a phase speed of approximately $40\,\mathrm{m\,s^{-1}}$. In an active avalanche experiment, these two sensors measured a near-surface, elliptical polarized vibration with a wavelength of 420 mm. The slightly dispersive waves generated by a booming avalanche were identified by Andreotti[13] as Rayleigh-Hertz modes of a surface wave. Bonneau, Andreotti, and Clement[14] stated that these waves would "correspond at the booming emission frequency f = 100 Hz to a phase velocity of $32\,\mathrm{m\,s^{-1}}$ and to a group velocity of $27\,\mathrm{m\,s^{-1}}$ for the mode n = 0". Gusev, Aleshin, and Tournat[15] and Aleshin, Gusev, and Tournat[16] analyzed guided surface acoustic modes and found that in case of very strong vertical velocity gradients, waves can turn back to the surface, resulting in confined waves and low velocity measurements. The fieldwork by Vriend *et al.*[8] used an array of 48 sensors and measured the non-dispersive wave speed of approximately $230\,\mathrm{m\,s^{-1}}$ during a booming event. Vriend *et al.*[8] argued that the sound amplification associated with booming results from constructive interference of a compressive P-wave within a natural waveguide in the top layer (depth of approximately 2 m) of the dune. Vriend *et al.*[17] measured the velocity increase with depth in this layer and found that, although the ray path

was slightly curved, the increase in vertical velocity was not large enough for the waves to turn around and they were still reflected from the interface. The frequency of the booming is set from the thickness of the waveguide and the P-wave speeds of the surficial layer of dry sand, the denser substrate half space, and the air above the surficial layer. Hence, the observed variation in booming frequency between seasons comes directly from changes in these physical parameters of the dune and does not depend on how the avalanche is initiated or the size of the sand grains. In addition, Vriend *et al.*[17] showed that the avalanche speed did not influence the sustained frequency and its harmonics, but only influenced the amplitude of the emission.

As described in the following section, the waves in the dune are generated by three different methods—the creation of a sand avalanche spanning several meters, short-duration shearing of a small area covered by a hand, and a pressure impulse on the dune directly. The difference in propagation speed and frequency content between booming and burping indicates that the two emissions and the waves propagating away from the source are fundamentally different. These measurements are not included in the papers by Vriend *et al.*[8] and Vriend *et al.*[17]. Besides providing a framework to understand the rich variety of desert sounds, these measurements show a clear relationship between the source mechanism and the subsequent generation of elastic and inelastic waves in a geological granular material. As described in the review by Michlmayr, Cohen, and Or[18], an understanding of wave propagation through granular materials provides a non-invasive framework for monitoring and characterizing soils and landscapes for potential failure zones or stressed geologic media.

II. SOURCE MECHANISM

To investigate the characteristics of booming and burping desert sounds, three methods are used to initiate the emission. The first method involves several people sliding in unison along a horizontal line down the slip face of the dune to create an avalanching of sand. The second method entails a local shearing of a thin layer of sand, approximately 50 mm deep, through the movement of a single hand. These first two methods induce an acoustic emission that is audible. The third method involves a millisecond pressure impulse using a 20 mm thick metal plate of 200 mm by 200 mm and mallet; this method is also used in the seismic refraction experiments found in Vriend *et al.*[8] and creates seismic waves

traveling in the desert dune. These three source events produce ground vibrations that are recorded by vertically oriented uniaxial geophones. In the first recording set up, illustrated in figure 2a, a finely spaced array of 12 vertical geophones, spaced either 0.25 or 1 m apart, is placed parallel to the crest. This set up records the acoustic emissions as pseudoplane waves perpendicular to the direction of the moving source. In the alternative set up, shown in figure 2b, 48 geophones, spaced 1 m apart, are used to investigate the wave speed in the downhill direction. The analysis of the geophone signals reveals information about the frequency characteristics of each of the source mechanisms and the wave velocities along the array.

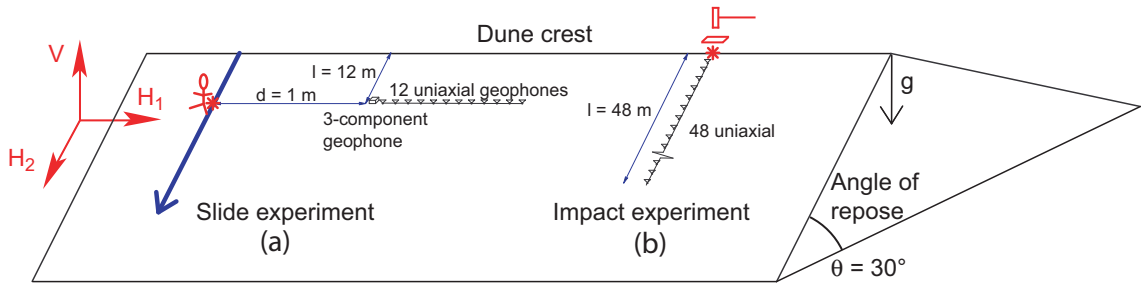


FIG. 2. (a) Arrangement of geophones (plane-wave) for the sliding experiment using 12 uniaxial geophones parallel to the crest with a spacing of 1 m and a three-component geophone at the position of the uniaxial geophone nearest to the source. The geophone array is located at a lateral distance d = 1 m from the source and at a distance l = 12 m from the crest. (b) Arrangement of geophones for the impact experiment using 48 uniaxial geophones perpendicular to the crest with a spacing of 1 m for a length of 48 m.

A. Sound induced by avalanching

Man-made or naturally induced sand avalanches on a dune slope at the angle of repose may produce the loud booming sounds. A natural avalanche occurs if sand, blown over the crest by the wind, deposits beyond the critical angle of repose and starts to slump spontaneously. Figure 3a shows a 4 s sample of geophone data, with a primary frequency of 85 Hz (± 4 Hz), deployed in the avalanching region at Eureka Dunes; a beating pattern is often apparent in the booming signal because of a slight mismatch of resonant frequencies. The waves generated by booming are also present at a depth of 200 mm, as evident from

the comparison in figure 3b between the vertical channel of a 3D geophone on the surface (black) and one buried at a depth of 200 mm (red). Although the amplitude of the buried sensor is slightly lower (a 30% drop), the frequency content is nearly identical.

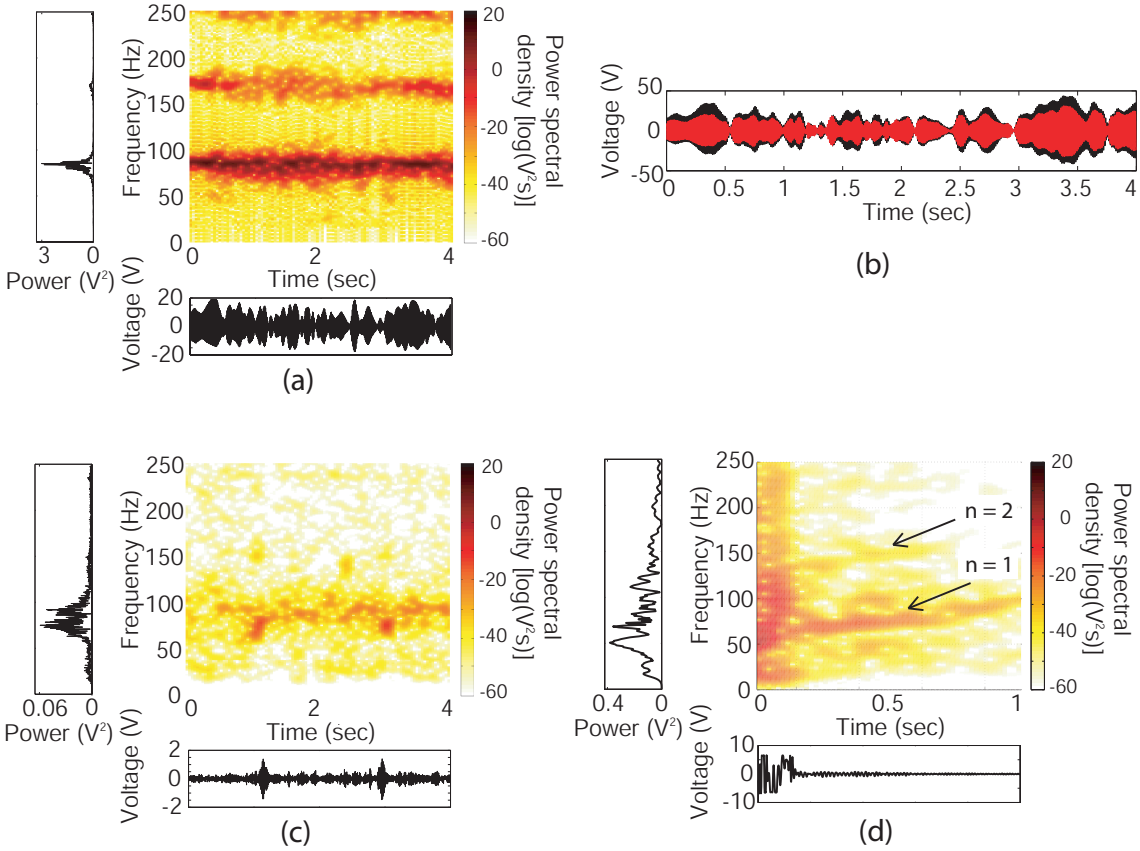


FIG. 3. Initiation mechanisms resulting in wave propagation at Eureka Dunes on 10/27/2007. Spectrogram, signal and power spectrum of the geophone recording created by the different initiation mechanisms: (a) creating a sand avalanche by sliding the sand regionally, (b) vertical raw signal of same slide recorded with one 3D geophone at the surface (black) and one buried at a depth of 200 mm (red), (c) shearing motion of sand grains locally by the movement of a hand and (d) pressure impulse due to a hammer impact on an aluminium plate. Note the scales for the amplitude and, for figure (d), time are different in each of the figures. The set up illustrated in figure 2a is used for the data in (a) through (c), while the set up sketched in figure 2b is used for the data in (d).

B. Sound induced by shearing

The signal shown in figure 3c contains short pulses (of approximately 0.1 s duration) of increasing and decreasing amplitude and results from direct shearing of sand by the movement of a hand. The velocity of the hand motion is approximately $0.25\,\mathrm{m\,s^{-1}}$, resulting in a shearing depth of approximately 50 mm and a shear rate estimated at $5\,\mathrm{s^{-1}}$. The sound stops abruptly when the applied shear ceases and is not sustained. The frequency content of the pulses is broadband and is centered around 76 ± 14 Hz. There is also a background signal present with a band around 94 Hz, but its magnitude is one order of magnitude lower than the short bursts and two orders of magnitude lower than the loud booming emission observed in figure 3a. The frequency of the low magnitude background signal is similar to the frequency measured for the booming sound.

C. Waves induced by pressure impulse

A hammer impact on an aluminum plate placed on the surface of the slip face produces a repeatable pressure impulse that creates broadband waves with frequencies up to 200 Hz. The impulse method does not simulate booming; instead it is a reproducible way to investigate the wave propagation and to measure the wave speed through the sand. On occasion as shown in figure 3d, the impact of the hammer, lasting only a tenth of a second, triggers an internal response that lasts up to a second. This response appears as a low magnitude main harmonic with at least one overtone, increasing from 70 to 95 Hz within one second. Direct shearing of sand is not involved in the generation of this response. This increase in frequency is likely a result of the propagating waves of the sudden impulse, moving downhill where the velocity structure of the dune increases its magnitude[8].

III. TYPES OF WAVES

Vriend *et al.*[8] investigated the compressional seismic velocities of the subsurface structure of a booming dune using refraction experiments involving equally-spaced geophones. A standard refractive analysis using the first arrivals revealed a layered structure along the upper part of the dune consisting of a near surface layer with waves travelling at a speed of $200 \pm 20\,\mathrm{m\,s^{-1}}$ on top of a faster half space with a speed of $350 \pm 30\,\mathrm{m\,s^{-1}}$. The sharp jump

in velocity is due to strong stratigraphical layering. A lithostatic increase in pressure does not account for the sharp layering observed in the measurements[17]. The lateral gradient of the seismic velocity in the downhill direction results from the down slope compaction of the sand.

Figure 4 shows the unscaled shot record of a seismic refraction experiment at Dumont Dunes on 05/29/2007, as illustrated in figure 2b. Waves are traveling in time from the impact source, represented by a star, at $t \sim 0$ and $r = 0$ along an array of 48 geophones. The first-arrival compressive P-wave has a speed α that increases from the start to the end of the line because of the increase in velocity with depth—the waves penetrate deeper into the dune for the farthest sensors. In addition to the compressive P-wave at speed α, the shot record shows a refracted body S-wave at speed β and a dispersed Rayleigh wave at phase speed c and group speed U. A refractive analysis, as highlighted in figure 4b, shows a near surface layer of $\alpha_1 = 180 \pm 20\,\mathrm{m\,s^{-1}}$ on top of a faster half space of $\alpha_2 = 300 \pm 30\,\mathrm{m\,s^{-1}}$.

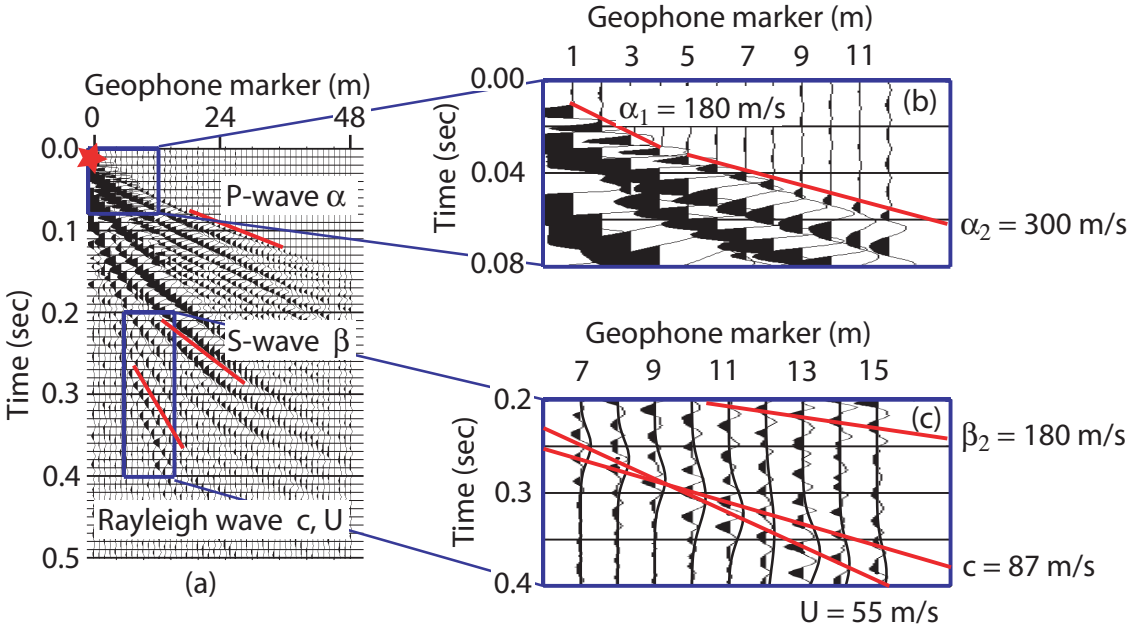


FIG. 4. (a) Shot record of the seismic refraction experiment, as sketched in figure 2b, of the Dumont Dune on 05/29/2007—the source is located at the star symbol. (b) Insert showing the first arrival P-waves with internal refractions resulting in distinct breaks in the slope where the velocity jumps from $180\,\mathrm{m\,s^{-1}}$ to $300\,\mathrm{m\,s^{-1}}$. (c) Insert illustrating the section of the data with the Rayleigh wave propagation—the phase velocity c and the group velocity U travel at distinct speeds.

A. Pressure waves

As shown in figure 5a with a closely-space geophone array (illustrated in figure 2a), the dilatational P-wave travels in radial direction as a propagating wave. Using the waveguide model as suggested by Vriend *et al.*[8], the pressure wave is a standing wave in z and a traveling wave in r, sandwiched between stiff boundaries at the top and bottom. As such, the wave function can be represented as a potential by a function of radial distance, r, depth, z, and time, t, as:

$$\phi(r, z, t) = A(\epsilon)\cos(k_\alpha z)J_n(k_\alpha r)e^{-i\omega t}. \tag{1}$$

with absorption coefficient ϵ and variable A. The wave propagates with phase velocity $\alpha = \omega/k_\alpha = \sqrt{(\lambda + 2\mu)/\rho}$, which is equal to the compressive P-wave speed. The wave equation in cylindrical polar coordinates can be solved using separation of variables (e.g. Kausel[19]) for r, z and t. The equation for the radial dependence leads to a Bessel equation, for which the solutions are Bessel functions of order n: $J_n(k_\alpha r)$. The depth and time dependence results in complex exponential expressions, for which the former can be simplified using the boundary conditions. At the interface on the surface ($z = 0$), traction and particle displacements are matched between the air and the upper layer of sand. At the bottom, the stiff boundary condition at $z = H$ with zero displacement is satisfied when $k_\alpha H = m\pi$, with integer m. The equation for the displacement u_r is obtained by summing all modes m such that[20]:

$$u_r(r, z, t) = Re\left[\sum_{m=0}^{\infty} \frac{B(\epsilon)}{r} U_m(t)\cos\left(\frac{m\pi z}{z_0}\right)e^{-i\omega t}\right], \tag{2}$$

with forcing function $U_m(t)$ and variable $B(\epsilon)$. In here, the far-field assumption has been made for the radial dependence, leading to an approximation of the Bessel function of $\sim 1/r$, with other variables incorporated in variable $B(\epsilon)$. Physically, one can visualize this as the energy of the first arrival P-wave spreading in a three-dimensional fashion from the source. Based on equation 2, the amplitude of the P-wave should be inversely related to the distance from the source, indicated by the star symbol. The magnitude is measured in situ for an impulse source; as found in figure 5b, the measured magnitude does decrease inversely with distance away from the source, $\sim 1/r$ and there is good correspondence between the measured and expected trends.

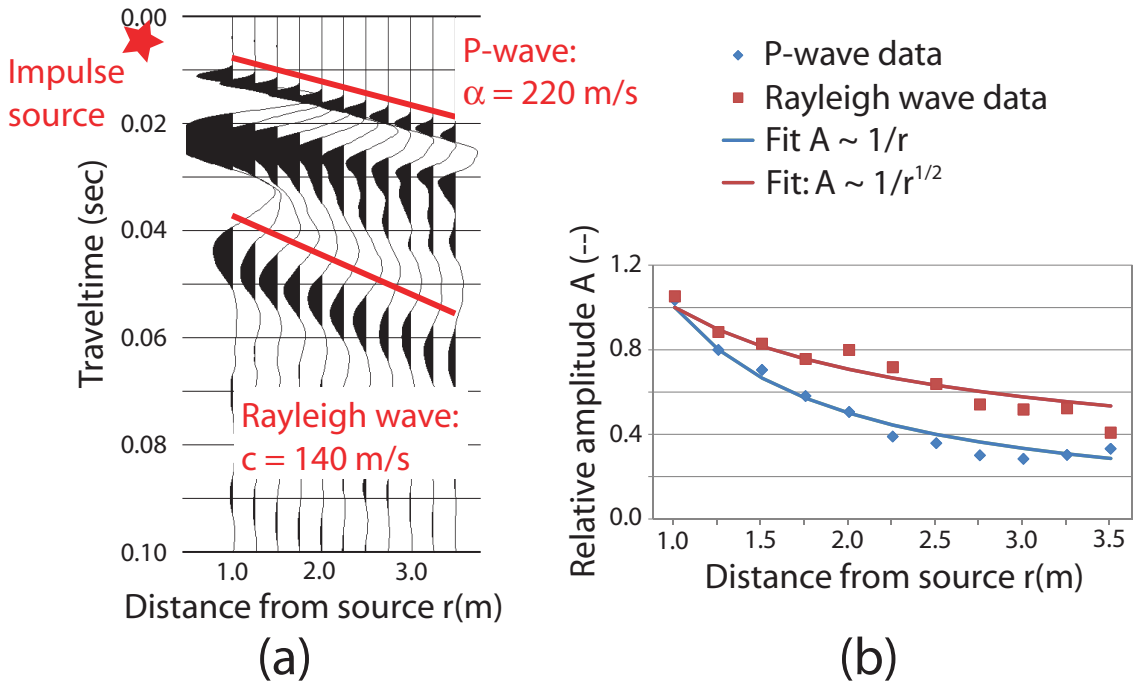


FIG. 5. Investigation of type of waves generated by a pressure impulse, as illustrated in figure 2a, on 06/01/2008 at Dumont Dunes with a finely spaced (0.25 m) geophone array. The source is located at the star symbol. (a) The body P-wave travels at a propagation velocity α of 220 m s^{-1}, while the surface Rayleigh wave travels slower at a phase speed c of 140 m s^{-1}, (b) normalized P-wave and Rayleigh wave amplitude as a function of the distance to the source r.

As illustrated in figure 4, the shear S-wave travels as a second-fastest wave packet after the P-wave. The S-waves show refracted arrivals on the shot record due to distinct jumps in velocity with depth, similar to those of the P-waves. The refraction shows a near surface layer with a slow direct S-wave at a speed $\beta_1 = 130 \pm 20$ m s^{-1} on top of a faster half-space velocity of $\beta_2 = 180 \pm 20$ m s^{-1}. Comparing this with the P-wave velocity, this results in a velocity ratio β/α of 0.60 – 0.72 in dune sand, which is in the range measured by Backrach, Dvorkin, and Nur [21] (0.64) for unconsolidated sand. Typical earth materials, modeled as a Poisson solid[22], have a lower ratio β/α of 0.58. The experiment uses vertical seismometers; thereby only records the vertical component (SV wave) and not the horizontal (SH) waves.

B. Rayleigh surface waves

The slowest wave is the dispersed Rayleigh surface wave; it is most pronounced for geophones seven through sixteen within the time interval of 0.2 – 0.4 s in figure 4 and more easily seen using closely-spaced geophones in figure 5. The Rayleigh wave is a surface wave and is confined to the upper part of the dune with the potential $\phi(r, z, t)$[23]:

$$\phi(r, z, t) = C(\epsilon)e^{-Fz}H_n(k_R r)e^{-i\omega t}, \tag{3}$$

with F a function dependent on the Rayleigh wave number k_R and variable C depending on the absorption coefficient ϵ. Furthermore, the surface Rayleigh wave speed $V_R = c = \omega/k_R \approx 0.9\beta$ for unconsolidated sand with Poisson's ratio $\nu = 0.15$[21]. The solution for the radial dependence leads to Hankel functions of order n: $H_n(k_R r)$. The energy of a surface Rayleigh wave spreads in a two-dimensional fashion with an exponential decay with depth. The equation for the displacement u_r is:

$$u_r(r, z, t) = Re\left[\frac{D(\epsilon)}{\sqrt{r}}U(t)e^{-Gz}e^{-i\omega t}\right], \tag{4}$$

with forcing function $U(t)$, variables D and G depending on the wavenumbers k_R, k_α and k_β and absorption coefficient ϵ. In the far-field approximation for the radial dependence, the Hankel function is approximated by $\sim 1/\sqrt{r}$, with other variables incorporated in variable D. The amplitude trend is inversely related to the square root of the distance to the source $\sim 1/\sqrt{r}$, which signifies amplitude decay in a cylindrical polar direction. Figure 5 shows good correspondence between the measured and predicted variation in amplitude with distance.

Dispersion is observed for the Rayleigh wave measured in the dune sand as shown in figure 4. The phase velocity is determined by tracing wave crests of the same phase. A Gaussian-shaped envelope is fitted to the signal of the Rayleigh wave, neglecting the influence of the earlier SV-wave and the background noise. The group velocity of the wave packet is found by analyzing the propagation of the Gaussian envelope. The group speed U is $55 \pm 5\,\mathrm{m\,s^{-1}}$ while the phase speed c is $87 \pm 6\,\mathrm{m\,s^{-1}}$.

The measured wave speeds can also be compared with values in the literature. The compressive wave speed for typical near-surface materials is $\alpha = 1000\,\mathrm{m\,s^{-1}}$ [24]. However, prior studies of seismic velocities in a granular material show that measured speeds in sand are much lower, due to the discrete nature of grains, local solid fraction and moisture be-

tween grains. Hardin and Richart[25] measured compressional and shear wave speeds of $\alpha \approx 330\,\mathrm{m\,s^{-1}}$ and $\beta \approx 135\,\mathrm{m\,s^{-1}}$ respectively at a confining pressures of 50,000 Pa, while Backrach, Dvorkin, and Nur[21] measured the compressional and shear wave speeds of unconsolidated sand at one meter depth as $\alpha \approx 230\,\mathrm{m\,s^{-1}}$ and $\beta \approx 145\,\mathrm{m\,s^{-1}}$. Brownell[26] noted that the preparation of the sand in laboratory experiments, and therefore its packing, strongly influenced the surface Rayleigh wave speed c. Brownell[26] and Bonneau, Andreotti, and Clement[27] measured values for the Rayleigh surface mode propagation of $c \approx 40 - 50\,\mathrm{m\,s^{-1}}$. In more recent studies by Bodet *et al.*[28] and Bergamo *et al.*[29] involving laboratory experiments using ultrasonic techniques on a granular subsurface, the longitudinal P mode featured velocities between 80 and $180\,\mathrm{m\,s^{-1}}$ depending on excitation frequency, while the slower vertical P-SV modes traveled at velocities below $120\,\mathrm{m\,s^{-1}}$.

The Rayleigh waves measured in the current study travel at similar speeds to the Rayleigh-Hertz guided surface wave identified by Bonneau, Andreotti, and Clement[14] as the main wave propagating the booming emission. More generally, the body and surface wave velocities measured in above mentioned laboratory studies compare well with the field results in this current study.

IV. FREQUENCY CONTENT

Figure 3 shows that the burping emission is broadband at a lower frequency (around $76 \pm 14\,\mathrm{Hz}$), while the booming emission is sharply defined in a narrow frequency band at $85 \pm 4\,\mathrm{Hz}$. In this section, the frequency content of the burping and booming emissions are further differentiated using band-pass filters.

As shown in the unfiltered signal of figure 6a, the fast P-waves, the slower S-waves, and the slowest Rayleigh waves are visible in the impulse experiment. However when the 25 – 60 Hz band pass filter is applied (figure 6b), the signal associated with the P-wave is diminished, but the signature associated with the S-waves ($\beta = 140 \pm 10\,\mathrm{m\,s^{-1}}$) and Rayleigh waves ($c = 87 \pm 6\,\mathrm{m\,s^{-1}}$) are apparent. Using the 60 – 100 Hz band pass filter (figure 6c), the filtered signal contains the P-wave ($\alpha = 240 \pm 20\,\mathrm{m\,s^{-1}}$) but not the S-wave or Rayleigh wave. Hence, these characteristics show that there is a clear distinction in frequency and propagation characteristics for the different type of waves. The difference in frequency generation is due to a finite source and the excitation function; similar observations are

found for Earth materials during earthquakes[22].

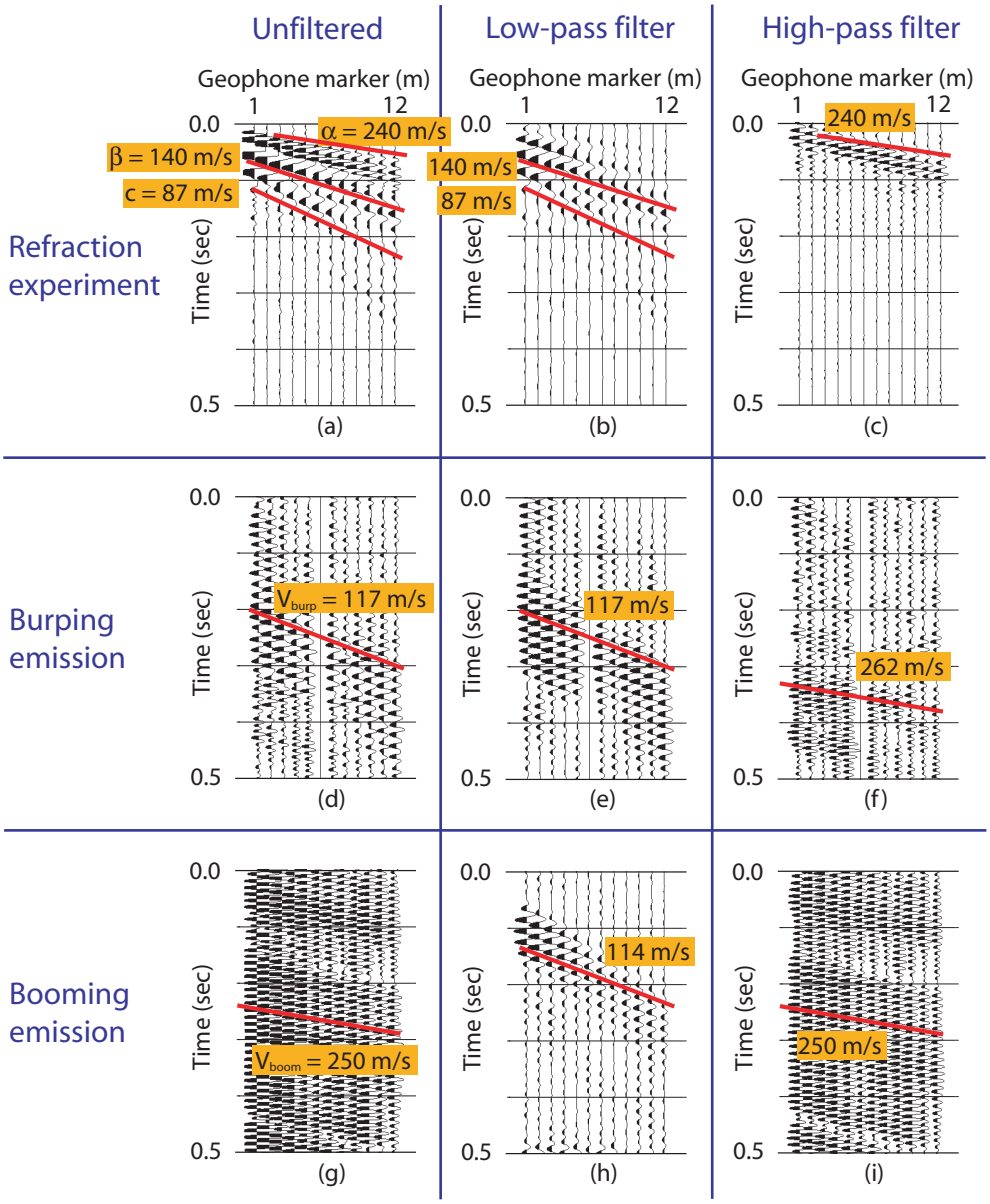


FIG. 6. Refraction experiments at Dumont dunes on 05/29/2007, as illustrated in figure 2a, showing (a) the raw signal; (b) after a 25 – 60 Hz band-pass filter is applied; (c) after a 60-100 Hz band-pass filter is applied. Burping experiments showing (d) the raw signal; (e) after a 25-60 Hz band-pass filter is applied; (f) after a 60 – 100 Hz band-pass filter is applied. Booming experiments showing (g) the raw signal; (h) after a 25 – 60 Hz band-pass filter is applied; (i) after a 60 – 100 Hz band-pass filter is applied. The amplitudes are different for each emission, as the low frequency (panel (e)) emission is dominant for the burping recording while the high frequency (panel (i)) is dominant for the booming recording. Channel six is malfunctioning in recording (d) through (f).

Figure 6d through f show 0.5 s of the burping recording generated by local shearing, similar to figure 3c. Both a fast-traveling high frequency (60 – 100 Hz) and a slow-traveling low-frequency component (25 – 60 Hz) are present. The slow wave travels at a velocity of $V_{burp,low} = 117 \pm 3\,\mathrm{m\,s^{-1}}$ in the low frequency range (figure 6e). The fast wave appears in the high frequency range in figure 6f and travels at a velocity of $V_{burp,high} = 262 \pm 8\,\mathrm{m\,s^{-1}}$. Comparing the amplitude of the two individual components shows that the fast body wave has a smaller amplitude and does not appear in the unfiltered figure 6d. The main component in the burping recording is propagating at a low speed ($V_{burp,low}$) and at a low frequency and is a pseudo-Rayleigh wave.

Figure 6g through i show 0.5 s of the booming recording, similar to figure 3a. Again, both a fast-traveling, high frequency (60 – 100 Hz) and a slow-traveling, low-frequency component (25 – 60 Hz) are present. The slow wave, traveling at a velocity $V_{boom,low} = 114 \pm 2\,\mathrm{m\,s^{-1}}$, is faint but distinguishable in figure 6h as a low-frequency wave of decreasing amplitude. The largest amplitude wave travels in the high frequency range at a velocity $V_{boom,high} = 250 \pm 5\,\mathrm{m\,s^{-1}}$ in figure 6i. Hence, the main signal in the booming recording is a fast-traveling, high-frequency P-wave at $V_{boom} = V_{boom,high} \approx 250\,\mathrm{m\,s^{-1}}$.

An analysis of frequency content and propagation speeds shows a clear distinction between burping and booming emission. The discrepancy between the speed of the burping emission $V_{burp} = 117\,\mathrm{m\,s^{-1}}$ and the Rayleigh wave velocity $c = 85\,\mathrm{m\,s^{-1}}$ is due to a difference in amplitude and is analyzed in section VI.

V. POLARIZATION CHARACTERISTICS

The analysis of behavior of particle motion provides a second method to distinguish between Rayleigh surface waves and P-waves[30]. Rayleigh surface waves have distinct polarization characteristics in which the particles describe a retrograde elliptical motion[22]. The wave motion of a body P-wave is in the direction of the wave propagation.

The three-component geophones are oriented by gravity-based leveling, but in post-processing the signals are converted to components of a coordinate system (V, H_1, H_2) parallel to the dune surface, as illustrated in figure 2. Frequency analysis shows the signal in each of the three components has the same frequency content for all emissions.

Plotting two different components of the geophone output creates a particle motion plot,

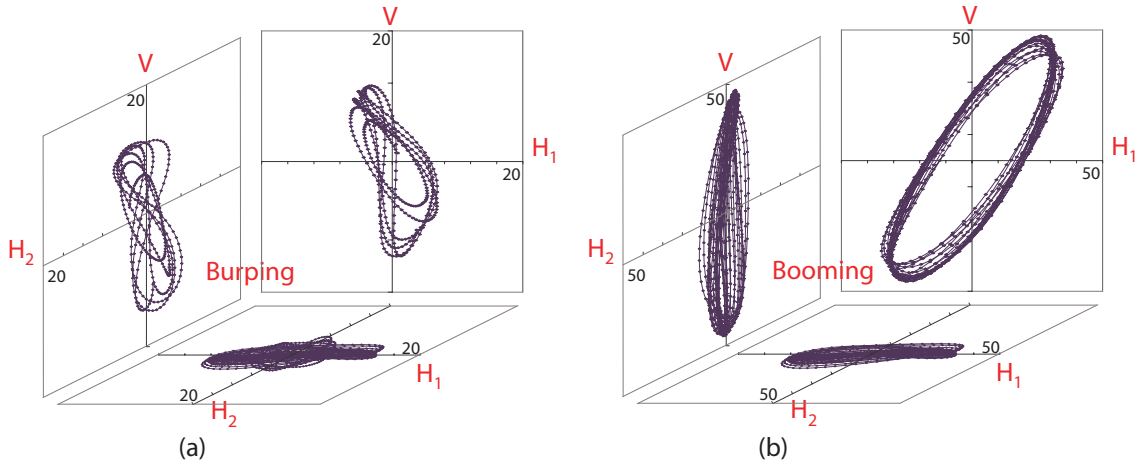


FIG. 7. Polarization plot of 3 component geophone recordings with a vertical (V), lateral horizontal (H_1) and longitudinal horizontal (H_2) component for the (a) burping and (b) booming recording on Eureka dunes on 10/27/2007. The burping recording (axis scaling $\pm$ 20) has a lower amplitude than the booming recording (axis scaling $\pm$ 50), as is evident from the raw data signal in figure 3.

which provides information about the character of the waves. The particle motion of the burping emission in figure 7a show a chaotic behavior without a repeatable pattern in any of the three projections. In contrast, the particle motion of the booming emission illustrated in figure 7b show repeatable ellipses in each of the three representations. The H_2-component perpendicular to the wave direction is small compared to the other two directions indicating that the out-of-plane motion associated with Love and/or SH-waves are not responsible for the emission. The major axis of the particle motion for the $V - H_1$ combination is not perpendicular to the surface, but tilts at an angle of 54°. Further analysis of the particle motion for the booming emission shows that the elliptical particle motion switches direction in the $V - H_1$ space after each instability as shown in figure 8.

A chaotic transition regime occurs when the booming fades for a fraction of a second. The displacement of a particle during a seismic booming wave shows a regular behavior in the V and H_1 directions. The repeatable particle path displays alternating prograde and retrograde tilted ellipses. The narrow ellipses have a maximum amplitude ratio V/H_1 of 1.4. The ratio corresponds to an angle of 54° with the horizontal as illustrated in figure 9. The critical angle θ_{cr} is 35° for a waveguide with characteristic velocities $\alpha_1 = 200\,\mathrm{m\,s^{-1}}$ and $\alpha_2 = 350\,\mathrm{m\,s^{-1}}$ [8] and corresponds to an angle of 55° with the horizontal. Therefore, the V and H_1 components map out the displacement of a particle in the waveguide during the

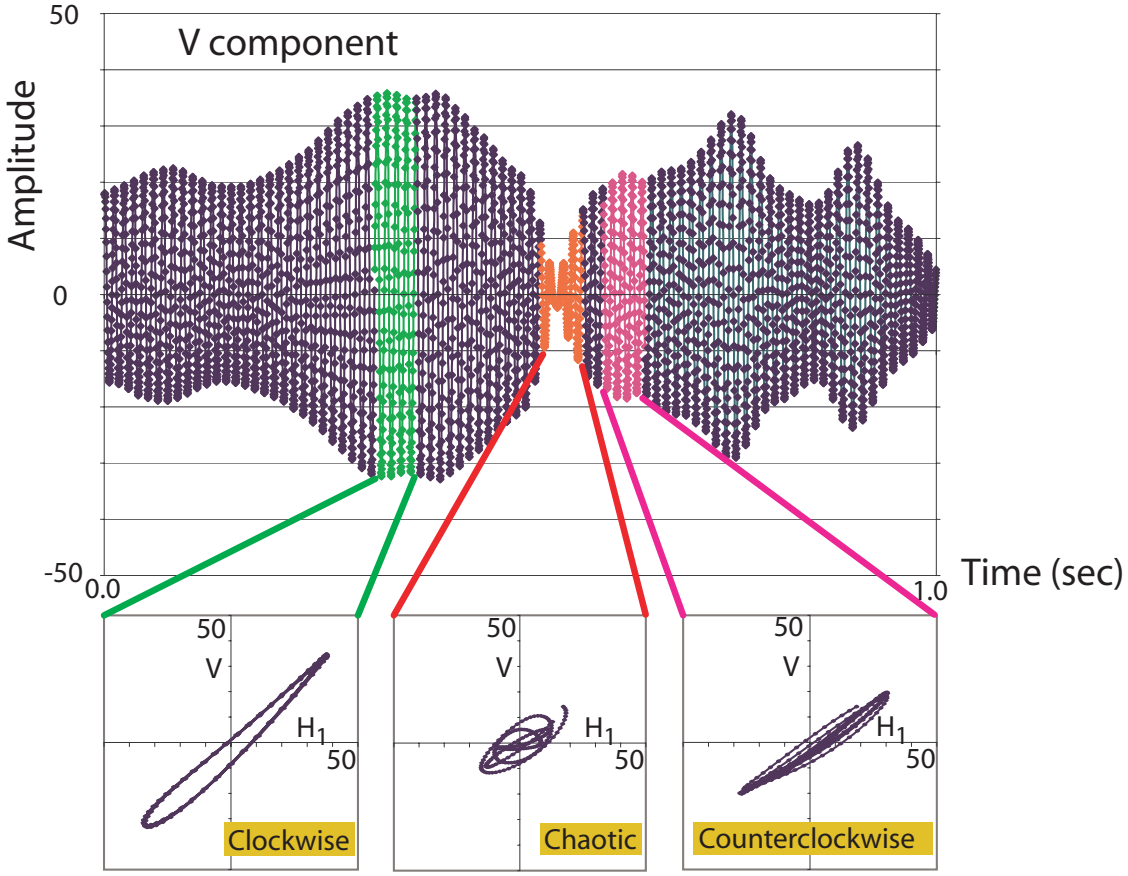


FIG. 8. Polarization characteristics of 1 s of the booming recording at Eureka Dunes on 10/27/2007. The original signal is the V-component, for which the beating of the signal is apparent. The orientation of the ellipse switches from clockwise to counterclockwise via a state in which chaotic movement is observed.

passing of a P-wave. A Rayleigh wave would have a retrograde elliptical motion with an amplitude of the vertical component at the surface of about 1.5 times the amplitude of the horizontal component and would not switch orientation. These characteristics of a Rayleigh wave are not consistent with the observed behavior of the wave responsible for the booming emission.

VI. DISPERSIVE AND NONLINEAR BEHAVIOR

The impulse seismic refraction experiment presented in figure 4 shows that the Rayleigh wave displays dispersive behavior with a phase speed $c = 87 \pm 6\,\mathrm{m\,s^{-1}}$ and a group speed $U = 55 \pm 5\,\mathrm{m\,s^{-1}}$. The burping emission, following the procedure outlined in section II B,

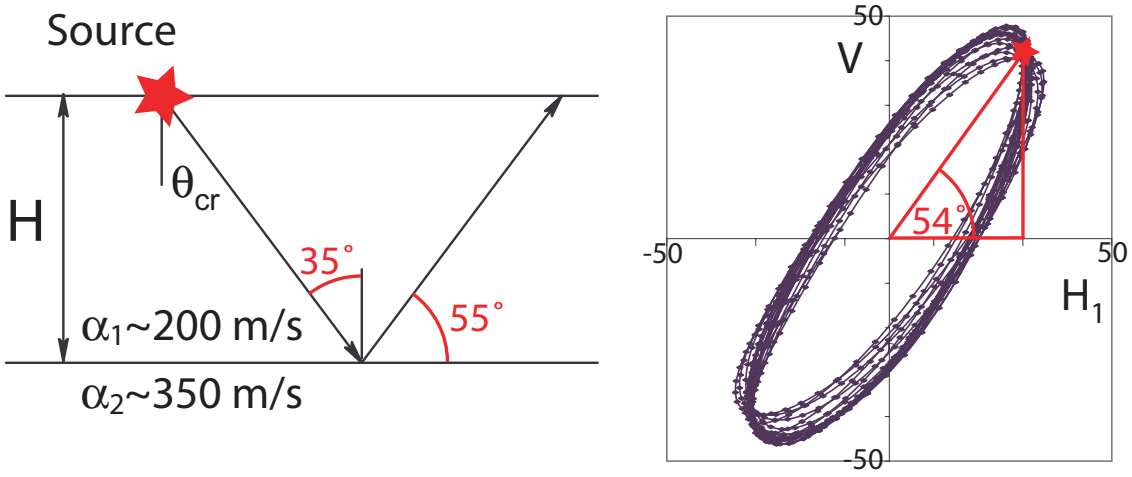


FIG. 9. Comparison between the orientation of the P-waves in a waveguide and the orientation of the V and H_1 component of the geophone.

features dispersive behavior as well, as observed in figure 6e. Geophone measurements from Dumont Dunes on 06/01/2008 (figure 10a) are used to characterize the dispersive behavior—this recording was chosen to analyze the burping signal because it is without significant background noise. Fitting a Gaussian shape to the signal gives a group speed $U = 52 \pm 5\,\mathrm{m\,s^{-1}}$. The duration of the burping pulse is not a function of distance to the source, but remains constant. The phase speed for the wavelets in figure 10a is found by tracing the crest of a waveform in time and space. This phase speed decreases strongly from $c = 148 \pm 14\,\mathrm{m\,s^{-1}}$ at maximum amplitude to $c = 110 \pm 6\,\mathrm{m\,s^{-1}}$ toward the beginning and end of the pulse where the amplitude is lower. The discrepancy between the group and phase speed indicates dispersion of the burping emission. The discrepancy between the phase speed of the wave in the burping experiment ($110 - 148\,\mathrm{m\,s^{-1}}$) and the Rayleigh wave in the refraction experiment ($c = 87\,\mathrm{m\,s^{-1}}$) is due to the nonlinear behavior of the wave propagation.

Figure 10b shows the phase speed of the waveform of the burp as a function of amplitude—the phase speed correlates directly to the amplitude, which is a strong indication of nonlinearity of the pulse. The phase speed is similar to a nonlinear Korteweg-de-Vries wave equation used for granular materials[31] in which the phase speed depends directly on the amplitude. The higher velocity of the center part of the pulse due to nonlinearity should produce a shock wave unless dispersive behavior counteracts the nonlinear effects. The exact

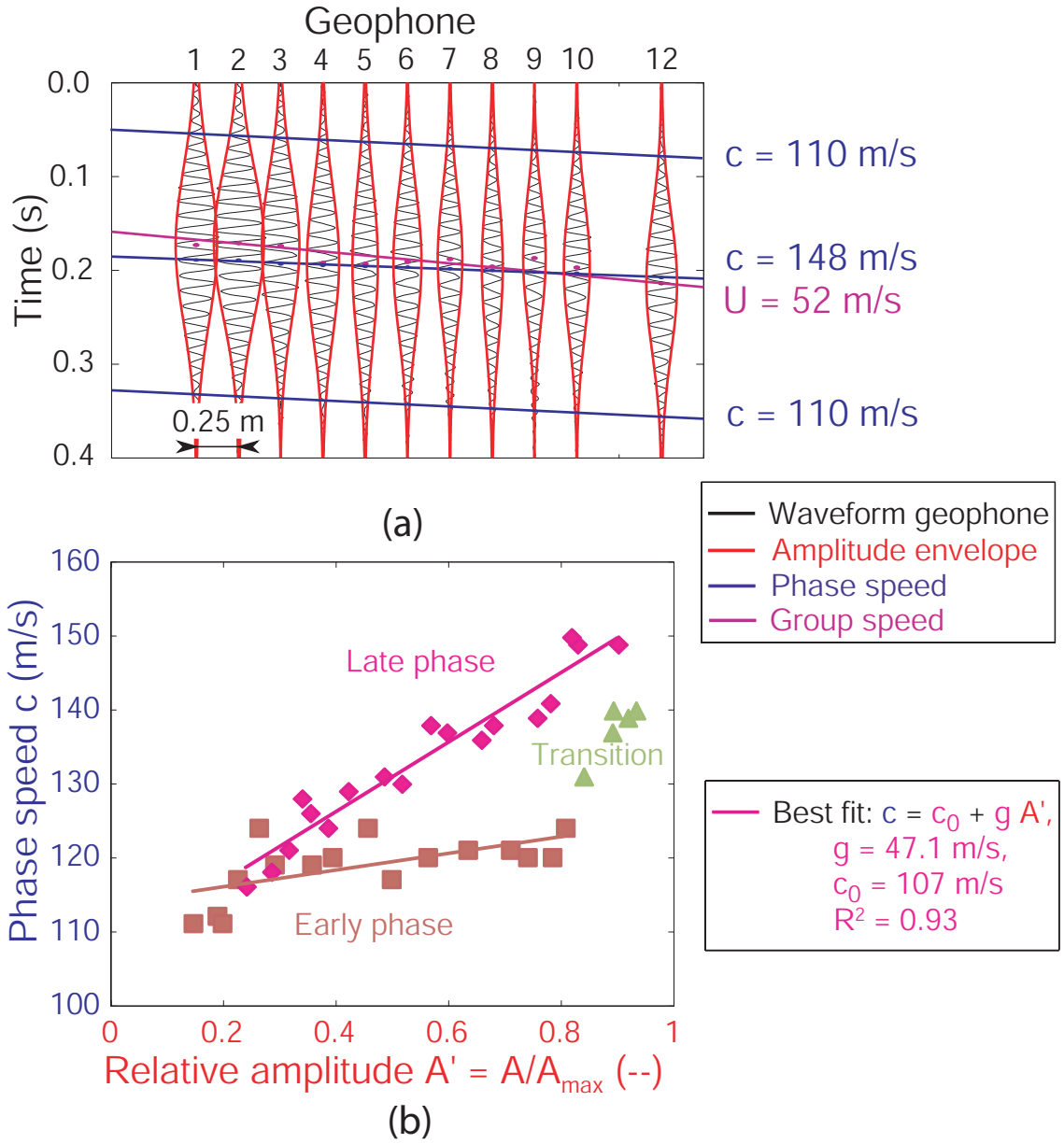


FIG. 10. Investigation of dispersive and nonlinear behavior of a burping emission recorded at Dumont Dunes on 06/01/2008: (a) Evolution of the burping pulse in space and time, indicating dispersive behavior, (b) correlation between the amplitude and the phase speed of individual wave crests, showing hysteresis between the early and late phase, indicating a nonlinear behavior. Twelve geophones were orientated as illustrated in figure 2a, geophone number 11 was malfunctioning.

interaction between nonlinearity and dispersive behavior for the burping emission remains an open question.

VII. DISCUSSION

In a granular material force chains across lengths scales on the order of tens of grain diameters transmit stresses that are easily broken and reformed[32]. On this small-scale grain-level, the interactions and deformations between grains are Hertzian, resulting in a non-linear relationship between stress and deformation[33]. At large scales that are orders of magnitude greater than the size of a grain, an effective medium approach can be used to determine the P- and S- wave speeds from the bulk properties of the materials. This distinction between scales and the link between the linear and non-linear transmission parallels the findings of the current study.

Jia, Caroli, and Velicky[34] investigated wave propagation in a granular bed and bridged the "effective medium" or averaged grain behavior, in terms of a coherent ballistic pulse, with the grain-size dependent wave propagation behavior resulting in a scattered signal. This dual and distinct behavior, highlighted as well in Michlmayr, Cohen, and Or[18] for acoustic emissions in stressed geologic granular media, parallels the binary behavior that has been outlined in this current study. Although there could be nonlinear sound generation within the source as well, the change with distance from the source as shown in figure 5b and figure 10 supports the argument that the nonlinear behavior is due at least in part to propagation and not just the generating source. The results of this field-based study demonstrates that the wave propagation behavior in a granular material can transition from nonlinear and dispersive surface wave behavior in the near-field to linear and non-dispersive body wave behavior in the far-field.

The local burping emission propagating across the surface shows dispersive and non-linear properties. The frequency of the resulting sound is broadly defined and depends on the direct influence of grain interaction and shearing. The narrow frequency spectrum of the larger-scale booming emission is selected from the broadband burping emission and propagates and amplifies within dune. Local inhomogeneities, due to individual grain-grain interactions, are averaged out and the resulting wave propagation produces a sharp and well-defined sound. This emission depends on mesoscale properties and creates an effective means to transmit monotonic waves.

In seismic surveys for oilfield exploration or earthquake investigations, the length-scales are usually much larger than in the current study. Even if the survey is done on a sandy

substrate, the "effective medium" response is recorded and the individual grain-interactions are usually not relevant. This study forms an excellent show-case to illustrate the dual behavior of the wave propagation when the scales reduce to a length where both the small-scale and the larger-scale meet.

Future work would need to involve a carefully controlled laboratory experiment that probes and investigates the transition between small-scale non-linear, dispersive wave propagation with the large-scale linear, non-dispersive wave propagation. This precise work could determine and quantify the exact nature of the nonlinear and dispersive effects that are observed in the burping emission.

VIII. CONCLUSIONS

This paper provides quantitative detail on the sound propagation in field studies to distinguish the type of waves that are responsible for the generation of the short burping and the sustained booming emission. The impulse seismic refraction studies show the existence of body P- and S-waves and surface Rayleigh waves in a granular material. Although both Rayleigh waves and P-waves are present during an acoustic emission on a sand dune, sustained booming is a result of body wave propagation and short-pulsed burping is related to Rayleigh surface wave propagation. The burping emission has a lower broadband frequency ($\sim$70 Hz) and travels at a slower velocity ($\sim$115 m s^{-1}). The prolonged booming emission propagates at a high frequency ($\sim$85 Hz) and at a higher velocity ($\sim$250 m s^{-1}).

Three component geophones show that for the booming emission the displacement of particles is in the same direction as the P-waves in the waveguide model. The particle paths are alternating prograde and retrograde, strongly tilting with the horizontal and not compatible with Rayleigh wave motion. The burping emission shows both dispersive and nonlinear characteristics, similar to Rayleigh surface wave behavior. Burping and booming emissions are different acoustic phenomena and are governed by different physical principles.

The low-speed (40 m s^{-1}), weakly dispersive signal that was obtained by Andreotti [13] is most likely a low amplitude direct measurement of Rayleigh wave behavior that is present within the dune and is consistent with measurements in this study; however, these waves are not significant in terms of the propagation of the booming signal. The booming emission is due to a P-wave type of behavior and is explained by the waveguide model as presented in

Vriend *et al.*[8].

ACKNOWLEDGMENTS

The authors would like to thank Dr. Chiara Daraio for the stimulating and fruitful discussions on wave propagation in a granular material. The help of Dr. Christopher Earls Brennen, Natalie Becerra, Dr. Angel Ruiz-Angulo, Dr. Erin Koos and many others, was essential during the field experiments at Dumont and Eureka dunes. Travel and equipment support for N. M. V. was provided through funding from the Pieter Langerhuizen Lambertuszoon Fonds. Raw data supporting figures 1, 3, 4, 5, 6, 7, 8 and 10 are available in the supporting information.

REFERENCES

[1]J. F. Lindsay, D. R. Criswell, T. L. Criswell, and B. S. Criswell, "Sound-producing dune and beach sands," Geological Society of America Bulletin **87**, 463–473 (1976).

[2]M. L. Hunt and N. M. Vriend, "Booming sand dunes," Annual Review of Earth and Planetary Sciences **38** (2010).

[3]M. Curzon of Kedleston, *Tales of travel* (reprinted in 1923 by Century Publishing, 1923).

[4]A. D. Lewis, "Roaring sands of the Kalahari Desert," South African Geographical Society **19**, 33 – 49 (1936).

[5]P. K. Haff, "Booming dunes," American scientist **74**, 376–381 (1986).

[6]F. Nori, P. Sholtz, and M. Bretz, "Booming sand," Scientific American **277**, 84–89 (1997).

[7]N. M. Vriend, M. L. Hunt, and R. W. Clayton, "Sedimentary structure of large sand dunes: examples from Dumont and Eureka dunes, California," Geophys. J. Int. **190**, 981–992 (2012).

[8]N. M. Vriend, M. L. Hunt, R. W. Clayton, C. E. Brennen, K. S. Brantley, and A. Ruiz-Angulo, "Solving the mystery of booming sand dunes," Geophysical Research Letters **34**, L16306 (2007).

[9]S. Dagois-Bohy, S. Courrech du Pont, and S. Douady, "Singing-sand avalanches without dunes," Geophysical Research Letters **39**, L20310 (2012).

[10]D. R. Criswell, J. F. Lindsay, and D. L. Reasoner, "Seismic and acoustic emissions of a booming dune," Journal of Geophysical Research **80**, 4963–4974 (1975).

[11]S. Douady, A. Manning, P. Hersen, H. Elbelrhiti, S. Protière, A. Daerr, and B. Kabbachi, "The song of the dunes as a self-synchronized instrument," Physical Review Letters **97**, 018002/1–018002/4 (2006).

[12]S. Dagois-Bohy, S. Ngo, S. Courrech du Pont, and S. Douady, "Laboratory singing sand avalanches," Ultrasonics **50**, 127–132 (2010).

[13]B. Andreotti, "The song of dunes as a wave-particle mode locking," Physical Review Letters **93**, 238001/1–238001/4 (2004).

[14]L. Bonneau, B. Andreotti, and E. Clement, "Surface elastic waves in granular media under gravity and their relation to booming avalanches," Physical Review E **75**, 016602 (2007).

[15]V. Gusev, V. Aleshin, and V. Tournat, "Acoustic waves in an elastic channel near the free surface of granular media," Phys. Rev. Lett. **96**, 214301 (2006).

[16]V. Aleshin, V. Gusev, and V. Tournat, "Acoustic modes propagating along the free surface of granular media," Journal of the Acoustical Society of America **121**, 2600–2611 (2007).

[17]N. M. Vriend, M. L. Hunt, R. W. Clayton, C. E. Brennen, K. S. Brantley, and A. Ruiz-Angulo, "Reply to comment on solving the mystery of booming sand dunes," Geophysical Research Letters **35**, L08307 (2008).

[18]G. Michlmayr, D. Cohen, and D. Or, "Sources and characteristics of acoustic emissions from mechanically stressed geologic granular media – a review," Earth-Science Reviews **112**, 97–114 (2012).

[19]E. Kausel, *Fundamental solutions in elastodynamics* (Cambridge University Press, 2006).

[20]N. H. Sleep and K. Fujita, *Principles of geophysics* (Blackwell Science, 1997).

[21]R. Backrach, J. Dvorkin, and A. M. Nur, "Seismic velocities and poisson's ratio of shallow unconsolidated sands," Geophysics **65**, 559–564 (2000).

[22]T. Lay and T. C. Wallace, *Modern global seismology* (Academic Press Limited, 1995).

[23]I. A. Viktorov, *Rayleigh and Lamb Waves – Physical Theory and Applications* (Plenum Press, New York, 1967).

[24]J. M. Reynolds, *An introduction to applied and environmental geophysics* (John Wiley and Sons, 1997).

[25]B. O. Hardin and F. E. Richart, "Elastic wave velocities in granular soils," Journal of the Soil Mechanics and Foundations division **89**, 33 – 65 (1963).

[26]P. H. Brownell, "Compressional and surface waves in sand - used by desert scorpions to locate prey," Science **197**, 479–482 (1977).

[27]L. Bonneau, B. Andreotti, and E. Clement, "Evidence of Rayleigh-Hertz surface waves and shear stiffness anomaly in granular media," Physical Review Letters **101**, 118001 (2008).

[28]L. Bodet, X. Jacob, V. Tournat, R. Mourgues, and V. Gusev, "Elasticity profile of an unconsolidated granular medium inferred from guided waves: Toward acoustic monitoring of analogue models," Tectonophysics **496**, 99–104 (2010).

[29]P. Bergamo, L. Bodet, L. Socco, R. Mourgues, and V. Tournat, "Physical modelling of a surface-wave survey over a laterally varying granular medium with property contrasts and velocity gradients," Geophysical Journal International **10.1093/gji/ggt521** (2014).

[30]J. E. Vidale, "Complex polarization analysis of particle motion," Bulletin of the Seismological Society of America **76**, 1393–1405 (1986).

[31]V. F. Nesterenko, *Dynamics of heterogeneous materials* (Springer New York, 2001).

[32]C. Liu and S. Nagel, "Sound in a granular material: Disorder and nonlinearity," Physical Review B **48**, 646–650 (1993).

[33]J. Lydon, K. R. Jayaprakash, D. Ngo, Y. Starosvetsky, A. F. Vakakis, and C. Daraio, "Frequency bands of strongly nonlinear homogeneous granular systems," Phys. Rev. E **88**, 012206 (2013).

[34]X. Jia, C. Caroli, and B. Velicky, "Ultrasound propagation in externally stressed granular media," Physical Review Letters **82**, 1863–1866 (1999).